

Probing the Colour Structure of the Top Quark Forward-Backward Asymmetry

Ben Gripaios^a, Andreas Papaefstathiou^b and Bryan Webber^a

^a*Cavendish Laboratory, J.J. Thomson Avenue, Cambridge, UK*

^b*Institut für Theoretische Physik, Universität Zürich, Switzerland*

E-mail: gripaios@hep.phy.cam.ac.uk, andreasp@physik.uzh.ch,
webber@hep.phy.cam.ac.uk

ABSTRACT: We point out that QCD coherence effects can help to identify the colour structure of possible new physics contributions to the anomalously large forward-backward asymmetry in top quark pair production. New physics models that yield the same inclusive asymmetry make different predictions for its dependence on the transverse momentum of the pair, if they have different colour structures. From both a fixed-order effective field theory approach and Monte Carlo studies of specific models, we find that an s -channel octet structure is preferred.

KEYWORDS: [Top Quark](#), [Hadronic Colliders](#), [QCD Phenomenology](#).

Contents

1. Introduction	1
2. Four-fermion interaction model	3
2.1 Operator basis	3
2.2 Born level cross-section	5
2.3 One gluon emission	6
2.4 Colour structure	6
2.5 Model results	6
3. Monte Carlo studies	11
3.1 Explicit new physics models	11
3.2 Monte Carlo implementation	11
3.3 Monte Carlo results	11
4. Conclusions	14
A. Amplitudes in the massless limit	16
A.1 One gluon emission	17
A.2 QCD amplitudes	19
A.3 Interference	20
A.4 Results	21

1. Introduction

The surprisingly large forward–backward asymmetry observed in the production of top quark pairs at the Tevatron [1–4] has given rise to many attempted explanations in terms of physics beyond the Standard Model (BSM): for recent reviews see for example [5–7]. New physics models seek to account for an asymmetry that rises with the top pair invariant mass and is about twice as large as the current best evaluations of the Standard Model prediction [8–10]. While the experimental and theoretical uncertainties are large enough that this discrepancy may eventually be resolved without new physics¹, it is important to constrain the BSM models with all possible relevant information. This has prompted us to consider the implications of the dependence of the asymmetry on the transverse momentum of the top pair, as reported by the CDF Collaboration [13].

¹Recent analyses of dileptonic top decays [11, 12] find lepton asymmetries less than two standard deviations from the Standard Model predictions.

The observed asymmetry is positive at low transverse momentum but falls and becomes negative at higher values. The leading-order QCD prediction has a similar behaviour but lies below the data. Again, it could be the case that further data and more complete Standard Model calculations would resolve this discrepancy. However, if new physics is invoked, then it should explain the transverse momentum dependence of the asymmetry as well as its invariant mass dependence.²

The tendency of the QCD contribution to the asymmetry to decrease with increasing transverse momentum of the top pair has a simple explanation in terms of QCD coherence [15], as was pointed out in [9, 16]. The contributing process $q\bar{q} \rightarrow t\bar{t}$ does not have an asymmetry at lowest order, but it has a colour structure that produces an asymmetry in higher orders. The s -channel gluon exchange means that colour flows predominantly from the incoming quark to the outgoing top, and anticolour from the incoming antiquark to the outgoing antitop. Thus there is more violent acceleration of the colour and anticolour sources in backward top production than in forward, leading to more QCD radiation in backward production, as depicted in Fig. 1. The emission of more radiation implies a larger recoil of the top pair, so that higher transverse momentum of the pair is correlated with a more backward top, and an asymmetry that decreases with increasing transverse momentum is generated. In contrast, an s -channel colour-singlet mechanism would imply no correlation between the amount of radiation and the production angle, as in Fig. 2, and therefore no correlation between the asymmetry and the transverse momentum of the pair.

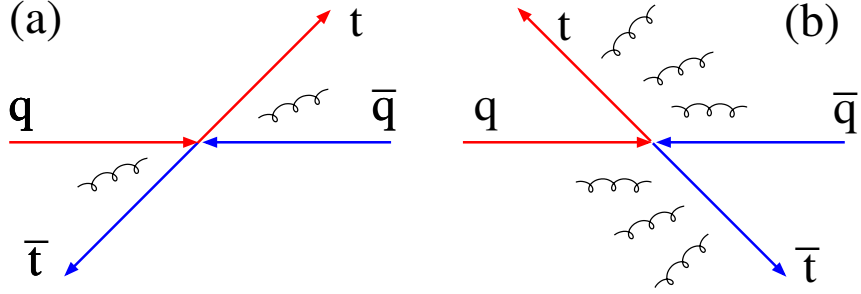


Figure 1: QCD radiation in $q\bar{q} \rightarrow t\bar{t}$ with an s -channel colour octet mechanism. There is less radiation when the top quark goes forwards (a) and more when it goes backwards (b).

Now if we apply the same logic to a new physics process that produces a positive asymmetry at lowest order, then we expect this asymmetry to be modified at non-zero transverse momentum by recoil effects if the process has an s -channel colour octet component. Backward top production will still be correlated with greater recoil momenta, so the asymmetry will be decreased relative to the lowest order. On the other hand, an s -channel singlet mechanism will not lead to any such change in the asymmetry relative to the lowest order.³

²In recent work [14] it was found that combining $t\bar{t}+0$ and 1-jet QCD NLO matrix elements with parton showers can give reasonable agreement with the transverse momentum dependence but not the invariant mass dependence.

³We should emphasise that we are referring here to the effects of real gluon emission, at strictly non-

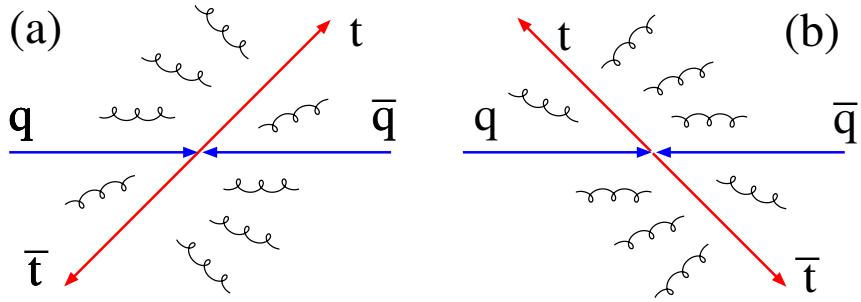


Figure 2: QCD radiation in $q\bar{q} \rightarrow t\bar{t}$ with an s -channel colour singlet mechanism. The amount of radiation is the same in forward (a) and backward (b) production.

To illustrate these ideas more quantitatively, we introduce in the following Section an effective four-fermion interaction, representing some mechanism beyond the Standard Model that can give rise to a forward-backward asymmetry at the Born level. We then examine the transverse momentum dependent asymmetry that would arise from gluon emission in such an interaction, contrasting the cases of s -channel octet and singlet colour structures and including interference with the QCD amplitude in the former. In each case we search for the values of the four-fermion couplings that give the best fits to the CDF data on the invariant mass and transverse momentum dependences of the asymmetry. In Section 3 we present results from the HERWIG++ event generator for two BSM models that illustrate the same points, and in Section 4 we summarize our conclusions. In the Appendix we present an analysis neglecting the top quark mass, which has the advantages that the relevant amplitudes can be given in a compact form and that the essential qualitative features of the predictions remain valid.

2. Four-fermion interaction model

2.1 Operator basis

We begin by asking which four-fermion operators generate an asymmetry at Born level. There are, *a priori*, infinitely many operators from which to choose, since operators of a given dimension in an effective field theory form a complex vector space. We are only interested in Lagrangian operators, which must be Hermitian and invariant under Lorentz and gauge transformations, and which span a real subspace. This subspace can be characterized by identifying a convenient basis.

Now, it is *not* sufficient to simply ask which of these basis elements generate an asymmetry at Born level: While the Lagrangian operators have the structure of a vector space, the asymmetries they result in (which are obtained from matrix elements *squared*) do not.

zero transverse momentum. At each perturbative order, there is a divergent virtual contribution at zero transverse momentum, and so the average asymmetry at non-zero values is not directly related to the inclusive asymmetry.

Therefore, to fully answer our question, we must consider the asymmetry that results from an arbitrary linear combination of the basis elements.

With this *caveat* acknowledged, we proceed to construct a basis of Lorentz and gauge-invariant (under $SU(3) \times U(1)$ symmetries, corresponding to QCD and electromagnetism⁴) dimension six operators involving a light quark-antiquark pair q, \bar{q} , and a heavy quark antiquark pair q', \bar{q}' , leaving aside the issue of hermiticity for the time being.

There are two possible $SU(3)$ colour structures, which correspond to decomposing each quark-antiquark pair into either a singlet or an octet representation. (Equivalently, each colour index of a given quark can be contracted with one of two anti-quarks, giving two linearly-independent operators.) It is these two possibilities that we hope to be able to discriminate using the distribution of the asymmetry in transverse momentum.

The analysis of Lorentz structures is simplified by the presence of Fierz identities, which allow us to interchange the two fermions in any 4-fermion operator.⁵ To be explicit, the most general form of the Fierz identity can be obtained by taking any basis $\{\Gamma^A\}$ for the vector space of complex, 4×4 matrices and writing the completeness relation on this space in the form $\delta_{ij}\delta_{kl} = \sum_A (\Gamma_A)_{il}(\Gamma^A)_{kj}$, where $\{\Gamma_A\}$ is the basis dual to $\{\Gamma^A\}$. From this one obtains the Fierz identity $\Gamma_{ij}^A \Gamma_{kl}^B = \sum_{C,D} \text{tr}(\Gamma^A \Gamma_D \Gamma^B \Gamma_C) \Gamma_{il}^C \Gamma_{kj}^D$. Using this identity, we can write all 4-fermion operators in the ordered form

$$(\bar{q}Mq)(\bar{q}'M'q'), \quad (2.1)$$

where M, M' are arbitrary complex, 4×4 matrices. (Proof: since bi-linears commute, we can, without loss of generality, write the one involving \bar{q} first; if this bi-linear involves q' , use a Fierz identity to exchange it with q .)

Next, we choose a particular basis $\{\Gamma^A\} = \{P_L, P_R, \gamma^\mu P_L, \gamma^\mu P_R, \sigma^{\mu\nu}\}$ for complex, 4×4 matrices. Out of these, we can form 10 Lorentz invariant four-fermion operators, namely those with Lorentz tensor combinations of the form $\{P_{L,R} \otimes P_{L,R}, \gamma^\mu P_{L,R} \otimes \gamma_\mu P_{L,R}, \sigma^{\mu\nu} \otimes \sigma^{\mu\nu}, \epsilon_{\mu\nu\sigma\rho} \sigma^{\mu\nu} \otimes \sigma^{\sigma\rho}\}$.

Finally, we must enforce the restriction of hermiticity. One can easily check that, amongst the four scalar combinations in the list, only $LL+RR$ and $LR+RL$ are Hermitian, reducing the dimension of the subspace of Lagrangian four-fermion operators to eight (or rather sixteen, once we include the two possible colour structures).

Having found a basis for the vector space of Lagrangian operators, we now ask which linear combinations of them can generate an asymmetry at Born level. This asymmetry can either arise directly from the BSM operator, or via interference with QCD. As we shall see below, operators built out of the (Lorentz) vector combinations $\gamma^\mu P_{L,R} \otimes \gamma_\mu P_{L,R}$ generate an asymmetry on their own (provided that the left and right couplings do not coincide), and in interfering with QCD if they are colour octets. These operators, moreover, are the ones obtained by integrating out the most interesting new physics candidates, such as an axigluon or a Z' . Operators built purely out of (Lorentz) scalar or tensor combinations

⁴Note that other authors [17, 18] restrict to operators symmetric under the full $SU(3) \times SU(2) \times U(1)$ group of the Standard Model.

⁵Since the two fermion bi-linears in such an operator commute, we can equivalently interchange the two anti-fermions.

do not interfere with QCD and do not generate an asymmetry on their own. Indeed, the only other combination of our basis elements that gives rise to an asymmetry involves the interference between scalar and tensor combinations. We do not pursue this possibility further here.

2.2 Born level cross-section

We thus consider a model in which a forward-backward asymmetry in $q\bar{q} \rightarrow q'\bar{q}'$ is produced by an effective four-fermion interaction of the form

$$\bar{q}\gamma^\mu(g_L P_L + g_R P_R)q \bar{q}'\gamma_\mu(g'_L P_L + g'_R P_R)q', \quad (2.2)$$

where q is massless and q' has mass m . Note that $g_{L,R}$ and $g'_{L,R}$ have dimension 1/mass.⁶ We treat all momenta as outgoing, i.e.

$$q(-p_1) + \bar{q}(-p_2) \rightarrow q'(p_3) + \bar{q}'(p_4), \quad (2.3)$$

and define $s_{ij} = (p_i + p_j)^2$. At Born level we have $s_{12} = s_{34} = s$, $s_{13} = s_{24} = t$ and $s_{23} = s_{14} = u$. Then the associated subprocess cross section is

$$\begin{aligned} \frac{d\sigma_{\text{BSM}}}{dt} = & \frac{1}{16\pi s^2} [(g_L^2 g_L'^2 + g_R^2 g_R'^2)(u - m^2)^2 + (g_L^2 g_R'^2 + g_R^2 g_L'^2)(t - m^2)^2 \\ & + 2(g_L^2 + g_R^2)g'_L g'_R m^2 s]. \end{aligned} \quad (2.4)$$

The corresponding QCD cross section has $g_{L,R} = g'_{L,R} = g_s$, a propagator factor of $1/s^2$ and a colour factor of $C_F/2N$. Thus

$$\frac{d\sigma_{\text{QCD}}}{dt} = \frac{g_s^4}{16\pi s^4} \frac{C_F}{N} [(u - m^2)^2 + (t - m^2)^2 + 2m^2 s]. \quad (2.5)$$

If, on the one hand, the BSM interaction is s -channel colour-singlet, the two contributions do not interfere and the forward and backward cross sections are

$$\begin{aligned} \sigma_{\text{F,B}}^{\text{sing}} = & \frac{1}{96\pi s^2} \sqrt{1 - \frac{4m^2}{s}} \left\{ [(g_L^2 + g_R^2)(g_L'^2 + g_R'^2)s^2 + 2C_F g_s^4/N] (s - m^2) \right. \\ & \left. + 6[(g_L^2 + g_R^2)g'_L g'_R s^2 + C_F g_s^4/N] m^2 \right\} \pm \frac{1}{128\pi} (g_L^2 - g_R^2)(g_L'^2 - g_R'^2)(s - 4m^2). \end{aligned} \quad (2.6)$$

If, on the other hand, the BSM contribution is s -channel colour-octet, then the colour factors are the same and the two contributions interfere:

$$\begin{aligned} \frac{d\sigma^{\text{oct}}}{dt} = & \frac{C_F}{32\pi s^4 N} \left\{ [(g_L g'_L s + g_s^2)^2 + (g_R g'_R s + g_s^2)^2] (u - m^2)^2 \right. \\ & + [(g_L g'_R s + g_s^2)^2 + (g_R g'_L s + g_s^2)^2] (t - m^2)^2 \\ & \left. + 2[(g_L^2 + g_R^2)g'_L g'_R s^2 + (g_L + g_R)(g'_L + g'_R)g_s^2 s + 2g_s^4] m^2 s \right\}, \end{aligned} \quad (2.7)$$

⁶Since the Lagrangian contains bi-linear functions of $g_{L,R}$ and $g'_{L,R}$, the physics will be invariant under a simultaneous change of sign of all of them. Similarly, since our observables are parity symmetric, cross-section formulæ will be invariant under $g_L^{(\prime)} \leftrightarrow g_R^{(\prime)}$.

giving

$$\begin{aligned}\sigma_{\text{F,B}}^{\text{oct}} = & \frac{C_F}{192\pi s^2 N} \sqrt{1 - \frac{4m^2}{s}} \left\{ [(g_L^2 + g_R^2)(g_L'^2 + g_R'^2)s^2 + 2(g_L + g_R)(g_L' + g_R')g_s^2 s + 4g_s^4] (s - m^2) \right. \\ & \left. + 6[(g_L^2 + g_R^2)g_L'g_R's^2 + (g_L + g_R)(g_L' + g_R')g_s^2 s + 2g_s^4] m^2 \right\} \\ & \pm \frac{C_F}{128\pi s N} [(g_L^2 - g_R^2)(g_L'^2 - g_R'^2)s + 2(g_L - g_R)(g_L' - g_R')g_s^2] (s - 4m^2). \quad (2.8)\end{aligned}$$

2.3 One gluon emission

The squared matrix elements for one-gluon emission in massive quark pair production are rather cumbersome, and we do not include them here. In the limit of negligible quark mass, helicity amplitude methods render the calculation much simpler, and it turns out that the important features of the effects we wish to study are manifest, so we discuss the massless case in some detail in the Appendix. To obtain the massive case results presented here,⁷ we revert to the old-fashioned approach *à la* Feynman, based on squared matrix elements rather than amplitudes, and averaged/summed over initial/final state helicities.⁸ We use FEYN CALC [20] to perform the more tedious Dirac algebra.

2.4 Colour structure

In the case of the four-fermion BSM interaction (2.2), for each combination of external helicities we can associate an amplitude $A^{(i)}$ with emission of a gluon from external line $i = 1, \dots, 4$. This is not a gauge-invariant procedure, but the full matrix element-squared can be represented as a sum of gauge-invariant combinations

$$\mathcal{M} = \sum_{i < j} C_{ij} |A^{(i)} - A^{(j)}|^2, \quad (2.9)$$

where the coefficients C_{ij} , averaged over initial and summed over final colours, are given in Table 1. The QCD expressions, and the QCD-BSM interference, can also be written in this form. The gauge-invariant combinations are given in the massless case by eqs. (A.25), (A.29) and (A.35) in the Appendix. We have checked that for pure QCD, our results for the massive case reproduce the expression given in [21].

We see from Table 1 that in the singlet case only the (12) and (34) terms contribute, and therefore we have the situation in Fig. 2, where the amount of QCD radiation is the same in forward and backward production. In the case of an octet interaction, on the other hand, the (13) and (24) terms are dominant, and there is more radiation in backward production, which correlates a higher transverse momentum of the heavy quark pair with a more negative asymmetry than that at Born level.

2.5 Model results

To study the viability of the four-fermion effective interaction (2.2) as a model for invariant mass and transverse momentum dependence of the $t\bar{t}$ forward-backward asymmetry

⁷Computation of the amplitudes in the massive case, both for real emission and the accompanying one-loop virtual diagrams, is reported in [19], but detailed results are not given.

⁸Doing so also provides an independent check of our results for $m = 0$.

ij	Singlet	Octet
12, 34	C_F	$-C_F/4N^2$
13, 24	0	$(C_F/2N)(C_F - 1/2N)$
14, 23	0	$C_F/2N^2$

Table 1: Colour factors C_{ij} for one gluon emission, for s -channel singlet or octet.

observed by the CDF Collaboration [13], we performed scans over the coupling constants $g_{L,R}, g'_{L,R}$, for both s -channel colour octet and singlet interactions, taking into account the interference with the QCD contribution in the octet case, both at the Born level and in one gluon emission.

The scans were restricted to coupling values between $+3$ and -3 TeV^{-1} , to limit disagreement with the invariant mass distribution of the cross section. We also restricted the scans to two dimensions by assuming equality of the light and heavy quark couplings, $g'_L = g_L$ and $g'_R = g_R$.⁹ A step size of 0.4 TeV^{-1} , with the reflection symmetry of the couplings, meant that 128 model points were scanned. At each model point, predictions were generated using 10^7 weighted Monte Carlo phase space points, and χ^2 values were computed for fits to the CDF data. We used the MSTW2008 NLO (68cl) parton density function set [22], with the strong coupling evaluated at the top mass, taken to be $m_t = 173 \text{ GeV}$.

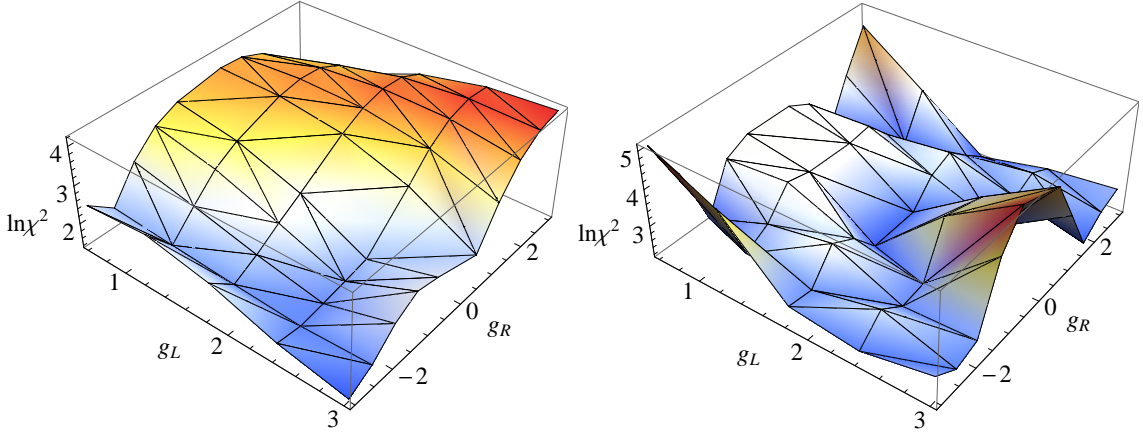


Figure 3: Values of $\ln \chi^2$ versus couplings $g_L = g'_L$ and $g_R = g'_R$ (units of TeV^{-1}) for colour octet (left) and colour singlet (right) four-fermion BSM interactions, compared to CDF data on the transverse momentum dependence of the asymmetry.

Figure 3 shows for example the χ^2 values for the fit to the transverse momentum dependence of the asymmetry, assuming either an s -channel colour octet (left) or singlet (right) four-fermion BSM interaction.¹⁰ Only the region $g_L > 0$ is shown, on account of the overall reflection symmetry of the couplings. We note, moreover, that for the colour

⁹In the octet case, we also performed a scan assuming $g'_L = -g_L$ and $g'_R = -g_R$, which is different owing to the interference with QCD, but the fits were less good.

¹⁰More generally, one could allow for an arbitrary linear combination of octet and singlet contributions.

Model	Best fit	g_L	g_R	$A_{\text{FB}}(M_{t\bar{t}})$	$A_{\text{FB}}(p_{Tt\bar{t}})$
Octet	$A_{\text{FB}}(M_{t\bar{t}})$	2.2	-0.2	$\chi^2 = 1.7$	$\chi^2 = 11.4$
	$A_{\text{FB}}(p_{Tt\bar{t}})$	3.0	-3.0	95.5	4.0
	Both	3.0	0.2	2.8	5.8
Singlet	$A_{\text{FB}}(M_{t\bar{t}})$	2.2	-0.6	$\chi^2 = 1.5$	$\chi^2 = 27.1$
	$A_{\text{FB}}(p_{Tt\bar{t}})$	3.0	1.8	12.1	8.7
	Both	1.8	-0.2	3.4	9.6
QCD LO				$\chi^2 = 27.4$	$\chi^2 = 45.6$

Table 2: Best fit couplings (in units of TeV^{-1}) and χ^2 values for different models and observables.

singlet interaction, there is approximate symmetry under $g_R = g'_R \rightarrow -g_R = -g'_R$, at fixed $g_L = g'_L$. Indeed, the diagrams we consider are invariant under $g_R \rightarrow -g_R$, at fixed g_L and *vice versa*. This is easily understood: our diagrams feature a single light quark line, along which helicity is conserved. In the singlet case, there is no interference with QCD, and so the sum of the powers of g_L and g_R in the matrix element squared must be two. The only such term which would not exhibit the claimed reflection symmetry in g_L and g_R separately is $g_L g_R$. This term could only arise via interference between two diagrams, one with a left-handed light quark line and one with a right-handed quark line. But such diagrams cannot interfere since the external light quarks in the two diagrams are in different helicity states. The analogous reflection symmetry in the heavy quark couplings g'_R and g'_L separately is broken by mass terms, which lead to helicity flips along quark lines and which account for the symmetry in Fig. 3 (right) not being exact. However, as we show in the Appendix, the neglect of mass terms in the matrix elements would not affect the qualitative features of our results.

Best-fit values of the couplings were found separately for the invariant mass and transverse momentum dependences, and for a simultaneous fit to both. The results are summarized in Table 2.

Fig. 4 shows the best-fit model results for the asymmetry as a function of $t\bar{t}$ invariant mass, for colour octet (left panel) and colour singlet (right panel) interactions, compared to the CDF data. In both cases one can obtain a good description of the data with reasonable values of the BSM couplings. However, the predictions for the dependence of the asymmetry on the $t\bar{t}$ transverse momentum (Fig. 5) are then very different, with the colour octet giving much better, albeit not perfect, agreement with the CDF data. In accord with the expectations discussed above, the octet interaction leads to an asymmetry that falls with increasing transverse momentum, while the singlet gives one that is larger and more constant, even slightly rising.

Although both the octet and singlet interactions can describe the invariant mass dependence well, neither gives a very good description of the separate forward and backward

Exchange of a colour triplet diquark in the t -channel, for example, leads to an equal admixture of octet and singlet in our effective theory. However, we shall see that the transverse momentum dependence qualitatively favours a pure octet.

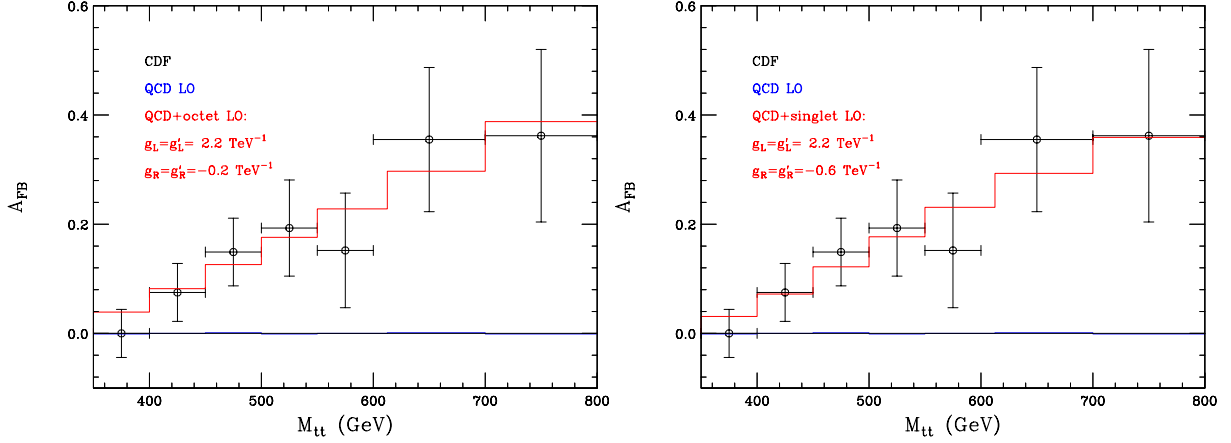


Figure 4: Best-fit model results for the forward-backward asymmetry as a function of the $t\bar{t}$ invariant mass, for colour octet (left) and colour singlet (right) four-fermion BSM interactions, compared to CDF data.

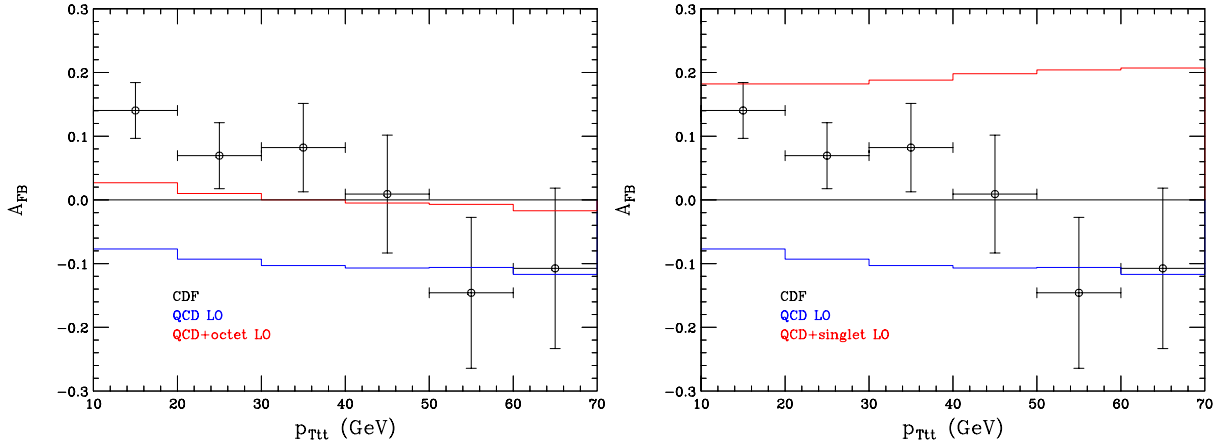


Figure 5: Model results for the forward-backward asymmetry as a function of the $t\bar{t}$ transverse momentum, for colour octet (left) and colour singlet (right) four-fermion BSM interactions, compared to CDF data. Coupling values as in Fig. 4.

production cross sections, Fig. 6, as both involve a BSM contribution that enhances the cross section at high mass. Nevertheless the octet gives significantly better agreement.

The fit of the singlet model to the transverse momentum dependence of the asymmetry can be improved by making the couplings larger and more left-right symmetric, but then the description of the invariant mass dependence becomes much worse, as shown in Fig. 7.

Overall, as other authors have noted [18, 23–27], the four-fermion BSM interaction has problems fitting the asymmetry data, but does better than leading-order QCD alone.

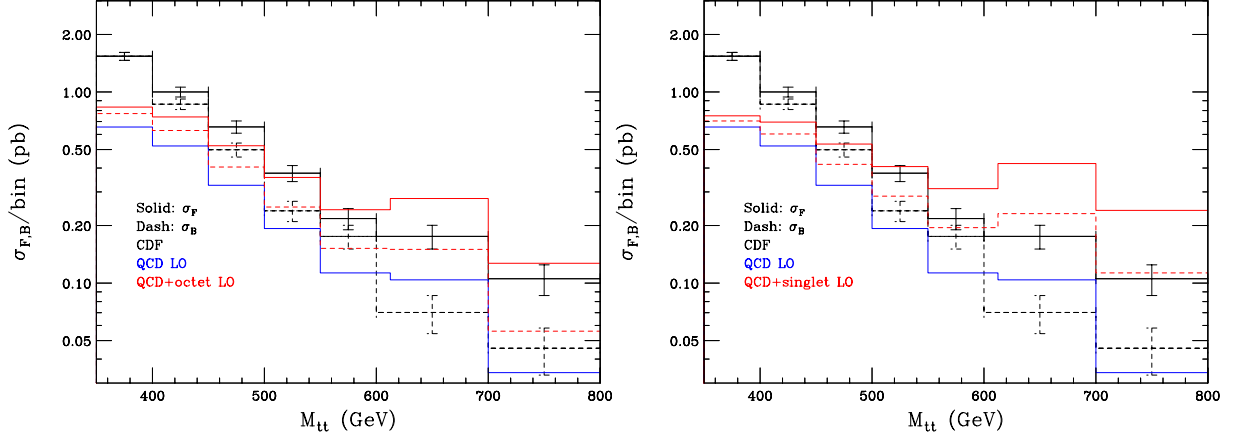


Figure 6: Model results for the forward (solid) and backward (dashed) $t\bar{t}$ cross sections, for colour octet (left) and colour singlet (right) four-fermion BSM interactions, compared to CDF data. Coupling values as in Fig. 4.

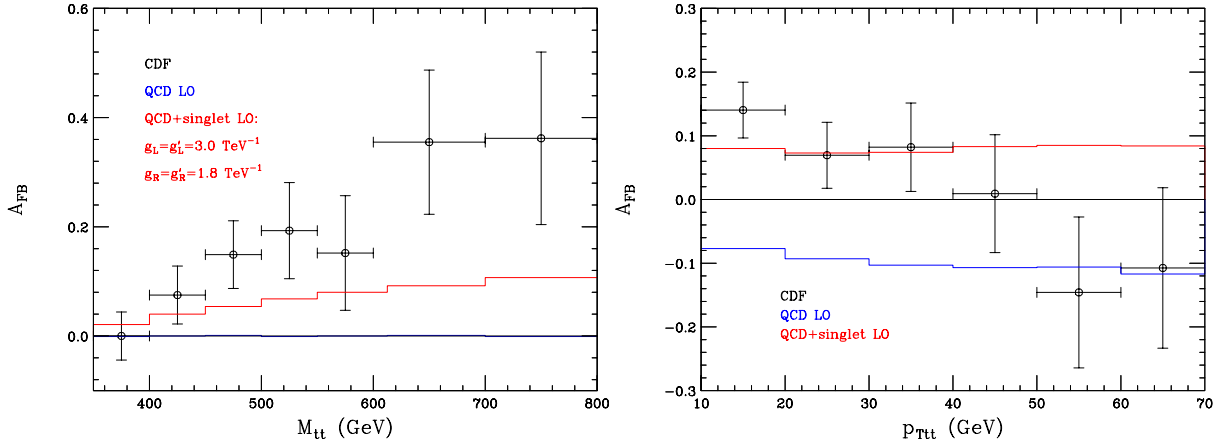


Figure 7: Best-fit singlet model results for the forward-backward asymmetry as a function of the $t\bar{t}$ transverse momentum, with the corresponding prediction for the invariant mass dependence, compared to CDF data.

We have found that an s -channel colour octet rather than singlet form of interaction is definitely preferred. This leaves open the possibility that QCD higher-order interactions could explain the data equally well.

3. Monte Carlo studies

3.1 Explicit new physics models

We extend our discussion by investigating the inclusion of explicit new resonances in conjunction with leading-order QCD. We focus on two models corresponding to the colour-singlet and colour-octet effective interactions investigated up to this point. The first is a Z' (Z -prime) colour-singlet vector boson whose Lagrangian contains interactions of the form:

$$(c_L^i \bar{q}_i \gamma^\mu P_L q_i + c_R^i \bar{q}_i \gamma^\mu P_R q_i) Z'_\mu, \quad (3.1)$$

where $c_{L,R}^i$ are the couplings of the Z' to the left- and right-handed quarks of flavour i , and Z'_μ is the Z' field. We will focus on the case where the only non-zero couplings are those to the up and top quarks, and couplings of the same chirality are equal ($c_L^i = c_L^j$, $c_R^i = c_R^j$, $i \neq j$). The second model we consider is that of a new colour-octet vector boson, which we will refer to as ‘axigluon’, \tilde{G} , whose Lagrangian contains interactions of the form:

$$g_s [\bar{q}_i T^A \gamma^\mu (c_L^i P_L + c_R^i P_R) q_i + \bar{t} T^A \gamma^\mu (c_L^t P_L + c_R^t P_R) t] \tilde{G}_\mu^A, \quad (3.2)$$

where g_s is the strong coupling constant of QCD, $c_{L,R}^i$ are the left- and right-handed couplings to $q_i \bar{q}_i$ (excluding the top quark), $c_{L,R}^t$ are the left- and right-handed couplings to $t \bar{t}$, the T^A ($A \in \{1, 8\}$) are the $SU(3)$ generators in the adjoint representation, and \tilde{G}_μ^A is the axigluon field. We will assume that the axigluon couplings to all the quark flavours (including the top quark) of the same chirality are equal and denote them by $c_{L,R}$.

The resulting effective four-fermion interactions will contain the heavy boson propagator. The propagator has a $\sim 1/M^2$ dependence on the boson mass, allowing us to make the identification $g \leftrightarrow c/M$ between the couplings of the effective theory and the explicit models, in the large M limit.

3.2 Monte Carlo implementation

Both of the above models are available in the **HERWIG++** event generator [28, 29]. **HERWIG++** constructs all the possible leading-order diagrams for $q\bar{q} \rightarrow t\bar{t}$, including the relevant interference between the colour-octet \tilde{G} and the QCD diagrams. An angular-ordered shower is added on top of the resulting matrix elements. Evidently, the finite gluon emission from internal QCD gluons is not included in this calculation. We also note that in Ref. [16] it was found that **HERWIG++** underestimates the effects of QCD coherence in the asymmetry.

A switch for limiting the shower to a single gluon emission either from the initial- or final-state partons has been added to the event generator and will be publicly available in the near future. In these studies we again use the MSTW2008 NLO (68cl) parton density function set [22]. We assume perfect reconstruction of the top and anti-top quarks, ignoring experimental effects.

3.3 Monte Carlo results

We performed fits to the CDF data equivalent to those described in Section 2.5. The scans were restricted to coupling values $c_{L,R} \in [-50.0, +50.0]$ in steps of width 2.0. We

Model	Best fit	c_L	c_R	$A_{\text{FB}}(M_{t\bar{t}})$	$A_{\text{FB}}(p_{Tt\bar{t}})$
Axigluon M = 800 GeV	$A_{\text{FB}}(M_{t\bar{t}})$	16.0	8.0	$\chi^2 = 3.8$	$\chi^2 = 3.7$
	$A_{\text{FB}}(p_{Tt\bar{t}})$	16.0	30.0	4.1	1.7
	Both	16.0	30.0	4.1	1.7
Axigluon M = 1600 GeV	$A_{\text{FB}}(M_{t\bar{t}})$	16.0	-6.0	$\chi^2 = 1.4$	$\chi^2 = 7.6$
	$A_{\text{FB}}(p_{Tt\bar{t}})$	14.0	-30.0	2.9	1.4
	Both	14.0	-30.0	2.9	1.4
Axigluon M = 2400 GeV	$A_{\text{FB}}(M_{t\bar{t}})$	34.0	-2.0	$\chi^2 = 1.8$	$\chi^2 = 3.8$
	$A_{\text{FB}}(p_{Tt\bar{t}})$	2.0	-32.0	2.2	1.9
	Both	2.0	-32.0	2.2	1.9
Z' M = 800 GeV	$A_{\text{FB}}(M_{t\bar{t}})$	4.0	2.0	$\chi^2 = 4.1$	$\chi^2 = 18.0$
	$A_{\text{FB}}(p_{Tt\bar{t}})$	32.0	-22.0	11.4	7.2
	Both	44.0	26.0	7.2	7.8
Z' M = 1600 GeV	$A_{\text{FB}}(M_{t\bar{t}})$	32.0	-12.0	$\chi^2 = 1.5$	$\chi^2 = 17.4$
	$A_{\text{FB}}(p_{Tt\bar{t}})$	10.0	22.0	5.3	5.8
	Both	4.0	-10.0	3.0	6.8
Z' M = 2400 GeV	$A_{\text{FB}}(M_{t\bar{t}})$	28.0	-2.0	$\chi^2 = 4.4$	$\chi^2 = 10.5$
	$A_{\text{FB}}(p_{Tt\bar{t}})$	36.0	-4.0	5.3	6.0
	Both	36.0	-4.0	5.3	6.0
QCD 1-gluon				$\chi^2 = 21.6$	$\chi^2 = 21.0$

Table 3: Monte Carlo best-fit couplings for explicit new physics models of a Z' and an axigluon and χ^2 values for different masses and different observables, restricting the shower to a single gluon emission.

considered heavy masses between $M = 800$ GeV and $M = 2400$ GeV in steps of 400 GeV. For each Monte Carlo point we generated 10^5 events, either restricting the shower to one gluon emission or with the full shower. Table 3 summarizes the results for the best fits for the one gluon emission case, for different mass values. Table 4 summarizes the equivalent results for the best fits for the full shower case. We also show the leading-order QCD result using the internal **HERWIG++** matrix elements, for comparison. The conclusions drawn from these results do not differ from those obtained by the use of the effective theory: Good descriptions of the data for $A_{\text{FB}}(M_{t\bar{t}})$ and $A_{\text{FB}}(p_{Tt\bar{t}})$ can be obtained in both the Z' and \tilde{G} models, for any mass value. There is a tendency for the fits to improve for larger boson masses and the full shower results fit the CDF data better than those including only a single gluon emission.

In Fig. 8 we show the best-fit model results for the asymmetry as a function of $t\bar{t}$ invariant mass, for boson masses $M = 1600$ GeV and for the full shower. The predictions for the $t\bar{t}$ transverse momentum distribution (Fig. 9) exhibit differences between the Z' and \tilde{G} similar to those observed in Fig. 5 between the singlet- and colour-octet effective four-fermion interactions: the axigluon leads to an asymmetry that falls with increasing $p_{Tt\bar{t}}$, whereas the singlet gives one that is roughly constant.

Model	Best fit	c_L	c_R	$A_{\text{FB}}(M_{t\bar{t}})$	$A_{\text{FB}}(p_{Tt\bar{t}})$
Axigluon M = 800 GeV	$A_{\text{FB}}(M_{t\bar{t}})$	30.0	18.0	$\chi^2 = 3.2$	$\chi^2 = 11.8$
	$A_{\text{FB}}(p_{Tt\bar{t}})$	28.0	50.0	4.6	11.2
	Both	12.0	22.0	3.7	11.3
Axigluon M = 1600 GeV	$A_{\text{FB}}(M_{t\bar{t}})$	10.0	-4.0	$\chi^2 = 1.5$	$\chi^2 = 7.9$
	$A_{\text{FB}}(p_{Tt\bar{t}})$	2.0	4.0	1.7	5.8
	Both	2.0	4.0	1.7	5.8
Axigluon M = 2400 GeV	$A_{\text{FB}}(M_{t\bar{t}})$	42.0	8.0	$\chi^2 = 1.3$	$\chi^2 = 6.5$
	$A_{\text{FB}}(p_{Tt\bar{t}})$	42.0	6.0	1.7	4.3
	Both	42.0	8.0	1.3	6.5
Z' M = 800 GeV	$A_{\text{FB}}(M_{t\bar{t}})$	30.0	16.0	$\chi^2 = 4.6$	$\chi^2 = 12.9$
	$A_{\text{FB}}(p_{Tt\bar{t}})$	6.0	-8.0	12.9	7.3
	Both	18.0	10.0	5.5	9.6
Z' M = 1600 GeV	$A_{\text{FB}}(M_{t\bar{t}})$	22.0	-10.0	$\chi^2 = 1.8$	$\chi^2 = 9.7$
	$A_{\text{FB}}(p_{Tt\bar{t}})$	24.0	-42.0	5.1	4.6
	Both	8.0	-16.0	2.3	6.2
Z' M = 2400 GeV	$A_{\text{FB}}(M_{t\bar{t}})$	46.0	-6.0	$\chi^2 = 1.6$	$\chi^2 = 7.8$
	$A_{\text{FB}}(p_{Tt\bar{t}})$	8.0	0.0	2.0	4.7
	Both	34.0	-2.0	1.7	5.0
QCD shower				$\chi^2 = 13.2$	$\chi^2 = 13.8$

Table 4: Monte Carlo best-fit couplings for explicit new physics models of a Z' and an axigluon and χ^2 values for different masses and different observables, with the full shower.

Model	mass (GeV)	c_L	c_R	$A_{\text{FB}}(M_{t\bar{t}})$	$A_{\text{FB}}(p_{Tt\bar{t}})$	$\sigma_{\text{F}}(M_{t\bar{t}})$	$\sigma_{\text{B}}(M_{t\bar{t}})$
Axigluon	2000	4.0	2.0	$\chi^2 = 5.3$	$\chi^2 = 8.5$	$\chi^2 = 9.7$	$\chi^2 = 27.8$
Z'	2400	0.0	2.0	3.7	8.9	20.8	62.3
QCD shower				13.2	13.8	15.7	59.6

Table 5: Monte Carlo best-fit couplings for the explicit new physics models of a Z' and an axigluon and χ^2 values found during the full scan. Fitted to all the differential distributions simultaneously, with the full shower. The QCD LO values are included for comparison.

Additionally, we performed simultaneous fits to all four CDF distribution, *i. e.* including the forward and backward differential cross sections with respect to the $t\bar{t}$ invariant mass. To obtain a fit that is better than leading-order QCD alone, it is necessary for the heavy boson mass in both models to lie in the region $M \gtrsim 1600$ GeV. The axigluon model gives a better fit to all distributions, particularly to the forward and backward differential cross sections, as was observed in Section 2.5. The values of the couplings for the best overall fits to all distributions are shown in Table 5 for both models, as well as QCD at leading order. Due to the constraints coming from the forward and backward cross sections, the couplings to the new bosons are required to be small.

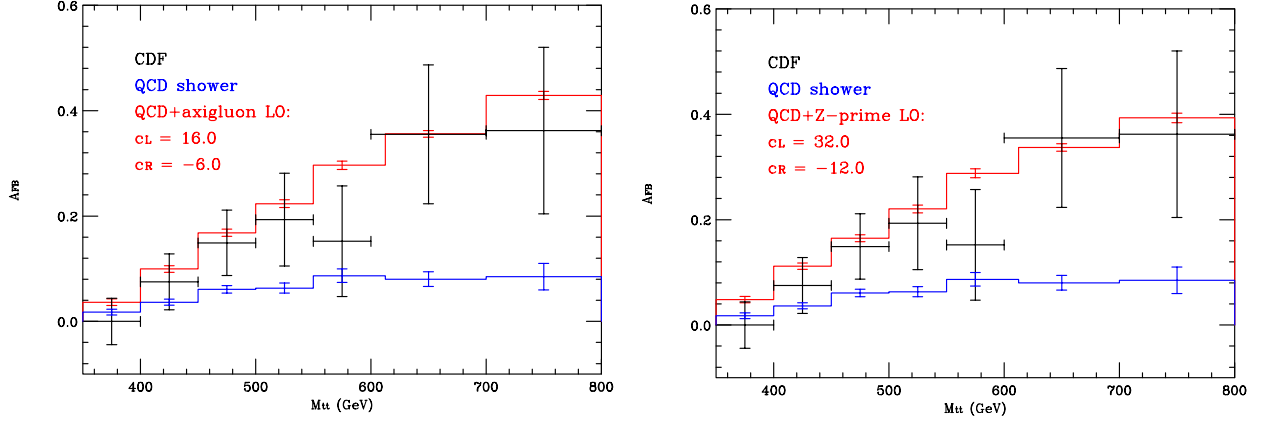


Figure 8: Monte Carlo best-fit model results for the forward-backward asymmetry as a function of the $t\bar{t}$ invariant mass, for the colour-octet axigluon (left) and colour-singlet Z' (right), compared to CDF data. The QCD shower result is included for comparison. The errors on the MC results are statistical.

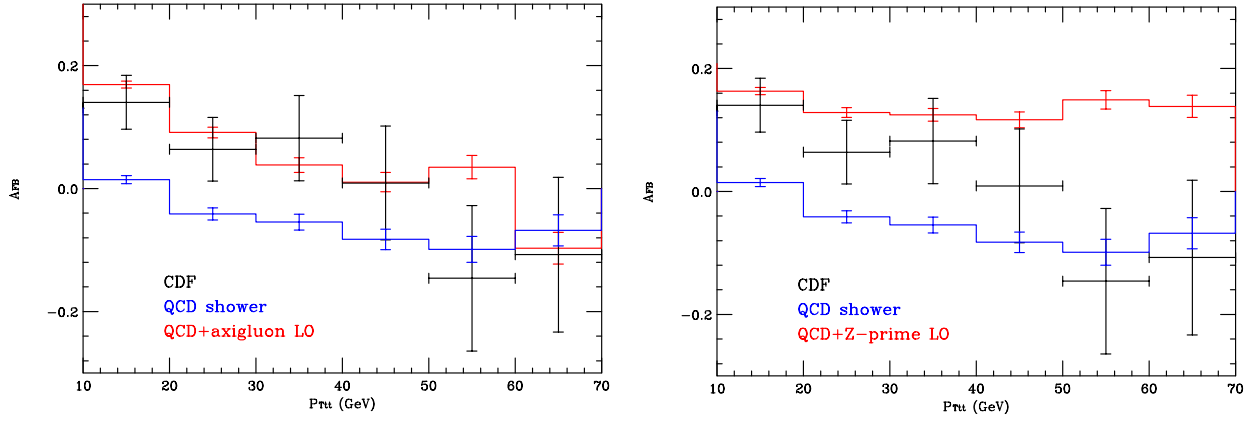


Figure 9: Monte Carlo best-fit model results for the forward-backward asymmetry as a function of the $t\bar{t}$ transverse momentum, for the colour-octet axigluon (left) and colour-singlet Z' (right), compared to CDF data. The QCD shower result is included for comparison. The errors on the MC results are statistical.

4. Conclusions

Our objective in this paper was not to propose a particular model for the top quark forward-backward asymmetry, nor indeed to advocate a BSM origin of the asymmetry at all. Our aim was rather to show, from various viewpoints, that the dependence of the asymmetry on the transverse momentum of the top pair provides additional information not available from the inclusive asymmetry alone. General features of the QCD dynamics of gluon emission from the Born process $q\bar{q} \rightarrow t\bar{t}$ ensure that mechanisms with the same inclusive asymmetry but different colour structures will exhibit different transverse momentum dependences. In

particular, when the initial state is a colour octet, the greater probability of gluon emission in backward top production implies a negative correlation between the asymmetry and the transverse momentum of the top pair. In the singlet state, on the other hand, there is no correlation between the gluon emission probability and the production angle and hence no such reduction of the asymmetry.

We illustrated these effects first with an effective four-fermion interaction that introduces an asymmetry at the Born level via different left- and right-handed couplings to light and/or top quarks. By computing the differential cross sections for one-gluon emission in the octet and singlet states, including the interference with pure QCD in the former, we showed that suitable choices of couplings could give good fits to the inclusive asymmetry in both cases. However, the corresponding transverse momentum dependences were then quite different, in accordance with our qualitative expectations, the CDF data favouring the octet state.

Whilst these conclusions seem qualitatively robust, it is important to note that our calculation of the transverse momentum distribution is effectively at the leading order of perturbation theory in QCD, and we expect that there might be significant corrections at next-to-leading-order, just as there are for pure QCD [30, 31].

We followed up this rather general fixed-order study with an investigation of specific models in the approximate all-orders framework provided by the `HERWIG++` Monte Carlo event generator. Comparing results for a massive colour octet ‘axigluon’ and a singlet Z' resonance decaying to $t\bar{t}$, both with variable left- and right-handed couplings, interfaced to `HERWIG++` parton showers, we found qualitatively similar results to those from the effective interaction. The Z' yields an asymmetry that is roughly constant while that for the axigluon falls with increasing transverse momentum, in better agreement with the CDF data. However, the axigluon mass needs to be high, above 1.6 TeV, and the couplings not too strong, in order for the fit to the forward and backward cross sections to be better than QCD alone.

Acknowledgements

BG acknowledges the support of the Science and Technology Facilities Council, the Institute for Particle Physics Phenomenology, and King’s College, Cambridge, and thanks Nordita for hospitality and support during part of this work. AP thanks Paolo Torrielli for useful discussions and acknowledges support by the Swiss National Science Foundation under contracts 200020-138206 and 200020-141360/1. BW thanks Kirill Melnikov and Gavin Salam for helpful discussions, acknowledges the support of a Leverhulme Trust Emeritus Fellowship, and thanks the Pauli Institute at ETH/University of Zurich for hospitality and support during part of this work.

A. Amplitudes in the massless limit

Neglecting masses, we use two-component spinor notation in the helicity basis

$$\gamma^\mu = \begin{pmatrix} 0 & \sigma^\mu \\ \bar{\sigma}^\mu & 0 \end{pmatrix}, \quad (\text{A.1})$$

where $\sigma^\mu = (1, \boldsymbol{\sigma})$, $\bar{\sigma}^\mu = (1, -\boldsymbol{\sigma})$. Left and right massless 2-spinors are represented as¹¹

$$\begin{aligned} u_L(p_k) &= v_R(p_k) = |k\rangle, & u_R(p_k) &= v_L(p_k) = |k\rangle, \\ u_L^\dagger(p_k) &= v_R^\dagger(p_k) = \text{sign}(p_k^0) \langle k|, & u_R^\dagger(p_k) &= v_L^\dagger(p_k) = \text{sign}(p_k^0) [k|. \end{aligned} \quad (\text{A.2})$$

Then

$$k \equiv p_k^\mu \sigma_\mu = |k\rangle \langle k|, \quad \bar{k} \equiv p_k^\mu \bar{\sigma}_\mu = |k\rangle [k|. \quad (\text{A.3})$$

Spinor products satisfy

$$\langle jk \rangle = -\langle kj \rangle, \quad [jk] = -\text{sign}(s_{jk}) \langle jk \rangle^* = -[kj] \quad (\text{A.4})$$

where $s_{jk} = 2p_j \cdot p_k$, so that

$$\langle jk \rangle [kj] = \text{sign}(s_{jk}) |\langle jk \rangle|^2 = s_{jk}. \quad (\text{A.5})$$

Also

$$[j\sigma^\mu k] = \text{sign}(s_{jk}) \langle k\bar{\sigma}^\mu j \rangle = \langle j\bar{\sigma}^\mu k \rangle^*. \quad (\text{A.6})$$

Then the relevant currents in the Born process (2.2) are

$$\begin{aligned} (\bar{q}\gamma^\mu q)_L &= \langle 2\bar{\sigma}^\mu 1 \rangle, & (\bar{q}\gamma^\mu q)_R &= \langle 1\bar{\sigma}^\mu 2 \rangle, \\ (\bar{q}'\gamma^\mu q')_L &= \langle 3\bar{\sigma}^\mu 4 \rangle, & (\bar{q}'\gamma^\mu q')_R &= \langle 4\bar{\sigma}^\mu 3 \rangle. \end{aligned} \quad (\text{A.7})$$

Applying the Fierz identity

$$\langle 1\bar{\sigma}^\mu 2 \rangle \langle 3\bar{\sigma}_\mu 4 \rangle = 2\langle 31 \rangle [24], \quad (\text{A.8})$$

we have helicity amplitudes

$$\begin{aligned} A_{LL} &= 2g_L g'_L \langle 32 \rangle [14], & A_{RL} &= 2g_R g'_L \langle 31 \rangle [24], \\ A_{LR} &= 2g_L g'_R \langle 42 \rangle [13], & A_{RR} &= 2g_R g'_R \langle 41 \rangle [23]. \end{aligned} \quad (\text{A.9})$$

Now $s_{31} = s_{24} = t$ and $s_{32} = s_{14} = u$. The BSM differential cross section is thus

$$\frac{d\sigma_{\text{BSM}}}{dt} = \frac{1}{16\pi s^2} [(g_L^2 g_R'^2 + g_R^2 g_L'^2) u^2 + (g_L^2 g_R'^2 + g_R^2 g_L'^2) t^2], \quad (\text{A.10})$$

in agreement with the massless limit of eq. (2.4). The QCD helicity amplitudes are the same, except that the couplings are $g_{L,R} = g'_{L,R} = g_s$, there is a propagator factor of $1/s_{12} = 1/s$, and the cross section has a colour factor of $C_F/2N$. It is therefore equally straightforward to verify the other equations in Sec. 2.2 in the massless limit.

¹¹The crucial sign factors are missing in some texts, which instead define, *e.g.* $k)^\dagger \equiv [k]$. The latter definition is inconsistent with the definition $k)[k \equiv 2\bar{\sigma}_\mu p_k^\mu$, as can be seen by comparing the traces $\text{tr } k)[k = \text{tr } k)k)^\dagger = k)^\dagger k)$, which is positive-definite, and $\text{tr } 2\bar{\sigma}_\mu p_k^\mu = 2p_k^0$, which can be of either sign in this all-states-outgoing formalism. We also include a sign factor in our phase convention, choosing $u_R(p_k) = \text{sign}(p_k^0) i\sigma^2 u_L^*(p_k)$.

A.1 One gluon emission

We can represent the polarization of a gluon with momentum p_5 by

$$\bar{\varepsilon}_L = \frac{\bar{\sigma}^\mu \langle 5\bar{\sigma}_\mu r \rangle}{\sqrt{2} [5r]}, \quad \bar{\varepsilon}_R = \frac{\bar{\sigma}^\mu \langle r\bar{\sigma}_\mu 5 \rangle}{\sqrt{2} \langle r5 \rangle}, \quad (\text{A.11})$$

where p_r is a lightlike reference vector not along p_5 . Then for emission from line 1 we have

$$\begin{aligned} \langle 2\bar{\sigma}^\mu 1 \rangle &\rightarrow \frac{g_s}{\langle 15 \rangle [51]} \langle 2\bar{\sigma}^\mu (1+5) \bar{\varepsilon} 1 \rangle \\ &= \frac{g_s}{\langle 15 \rangle [51]} (\langle 2\bar{\sigma}^\mu 1 \rangle \langle 1\bar{\varepsilon} 1 \rangle + \langle 2\bar{\sigma}^\mu 5 \rangle \langle 5\bar{\varepsilon} 1 \rangle). \end{aligned} \quad (\text{A.12})$$

Now, using Fierz again,

$$\begin{aligned} \langle 1\bar{\varepsilon}_L 1 \rangle &= \sqrt{2} \langle 51 \rangle [1r] / [5r], \quad \langle 1\bar{\varepsilon}_R 1 \rangle = \sqrt{2} \langle r1 \rangle [15] / \langle r5 \rangle, \\ \langle 5\bar{\varepsilon}_L 1 \rangle &= \sqrt{2} \langle 55 \rangle [1r] / [5r] = 0, \quad \langle 5\bar{\varepsilon}_R 1 \rangle = \sqrt{2} \langle r5 \rangle [15] / \langle r5 \rangle = \sqrt{2} [15]. \end{aligned} \quad (\text{A.13})$$

Hence, denoting the amplitude for emission of a gluon of helicity h'' from line j by $A_{hh',h''}^{(j)}$,

$$\begin{aligned} A_{LL,L}^{(1)} &= \sqrt{2} g_L g'_L g_s \frac{[1r]}{[15][5r]} \langle 2\bar{\sigma}^\mu 1 \rangle \langle 3\bar{\sigma}_\mu 4 \rangle \\ &= 2\sqrt{2} g_L g'_L g_s \frac{\langle 32 \rangle [14] [1r]}{[15][5r]} \equiv 2\sqrt{2} g_L g'_L g_s L(1234). \end{aligned} \quad (\text{A.14})$$

Similarly

$$\begin{aligned} A_{LL,R}^{(1)} &= \sqrt{2} g_L g'_L g_s \frac{g_s}{\langle 51 \rangle} \left(\frac{\langle r1 \rangle}{\langle r5 \rangle} \langle 2\bar{\sigma}^\mu 1 \rangle + \langle 2\bar{\sigma}^\mu 5 \rangle \right) \langle 3\bar{\sigma}_\mu 4 \rangle \\ &= 2\sqrt{2} g_L g'_L g_s \frac{\langle 32 \rangle}{\langle 51 \rangle} \left(\frac{\langle r1 \rangle}{\langle r5 \rangle} [14] + [54] \right) \equiv 2\sqrt{2} g_L g'_L g_s R(1234). \end{aligned} \quad (\text{A.15})$$

For emission from line 2

$$\begin{aligned} \langle 2\bar{\sigma}^\mu 1 \rangle &\rightarrow \frac{g_s}{\langle 25 \rangle [52]} \langle 2\bar{\varepsilon} (2+5) \bar{\sigma}^\mu 1 \rangle \\ &= \frac{g_s}{\langle 25 \rangle [52]} (\langle 2\bar{\sigma}^\mu 1 \rangle \langle 2\bar{\varepsilon} 2 \rangle + \langle 5\bar{\sigma}^\mu 1 \rangle \langle 2\bar{\varepsilon} 5 \rangle) \end{aligned} \quad (\text{A.16})$$

and

$$\begin{aligned} \langle 2\bar{\varepsilon}_L 2 \rangle &= \sqrt{2} \langle 52 \rangle [2r] / [5r], \quad \langle 2\bar{\varepsilon}_R 2 \rangle = \sqrt{2} \langle r2 \rangle [25] / \langle r5 \rangle, \\ \langle 2\bar{\varepsilon}_L 5 \rangle &= \sqrt{2} \langle 52 \rangle, \quad \langle 2\bar{\varepsilon}_R 5 \rangle = 0. \end{aligned} \quad (\text{A.17})$$

Therefore

$$\begin{aligned} A_{LL,L}^{(2)} &= 2\sqrt{2} g_L g'_L g_s \frac{[14]}{[25]} \left(\frac{[2r]}{[5r]} \langle 32 \rangle + \langle 35 \rangle \right) = 2\sqrt{2} g_L g'_L g_s R^*(2143), \\ A_{LL,R}^{(2)} &= 2\sqrt{2} g_L g'_L g_s \frac{[14] \langle 32 \rangle \langle r2 \rangle}{\langle 52 \rangle \langle r5 \rangle} = 2\sqrt{2} g_L g'_L g_s L^*(2143). \end{aligned} \quad (\text{A.18})$$

hh', h''	1	2	3	4	g	Term
LL, L	$L(1234)$	$R^*(2143)$	$R^*(3412)$	$L(4321)$	$G(1234)$	s_{14}^2
LL, R	$R(1234)$	$L^*(2143)$	$L^*(3412)$	$R(4321)$	$G^*(2143)$	s_{23}^2
LR, L	$L(1243)$	$R^*(2134)$	$L(3421)$	$R^*(4312)$	$G(1243)$	s_{24}^2
LR, R	$R(1243)$	$L^*(2134)$	$R(3421)$	$L^*(4312)$	$G^*(2134)$	s_{13}^2
RL, L	$R^*(1243)$	$L(2134)$	$R^*(3421)$	$L(4312)$	$G(2134)$	s_{13}^2
RL, R	$L^*(1243)$	$R(2134)$	$L^*(3421)$	$R(4312)$	$G^*(1243)$	s_{24}^2
RR, L	$R^*(1234)$	$L(2143)$	$L(3412)$	$R^*(4321)$	$G(2143)$	s_{23}^2
RR, R	$L^*(1234)$	$R(2143)$	$R(3412)$	$L^*(4321)$	$G^*(1234)$	s_{14}^2

Table 6: Helicity amplitudes for one gluon emission. Column i shows the function for emission from line i , to be multiplied by the coupling factor $g_h g_{h'}' g_s$. Column g refers to the QCD emission from the internal gluon line. The final column shows the associated term in Eq. (A.26).

In fact, all the contributions to the helicity amplitudes can be expressed in terms of the two functions L and R , defined by Eqs. (A.14) and (A.15) respectively, as shown in Table 6.

The colour factor for the various contributions to the matrix element squared are given in Table 1. For the colour-singlet case the matrix elements squared thus take the form

$$\mathcal{M}_{hh', h''}^{\text{sing}} = C_F \left(|A_{hh', h''}^{(1)} - A_{hh', h''}^{(2)}|^2 + |A_{hh', h''}^{(3)} - A_{hh', h''}^{(4)}|^2 \right). \quad (\text{A.19})$$

Consider for example the case $hh', h'' = LL, L$. We have

$$\begin{aligned} A_{LL, L}^{(1)} - A_{LL, L}^{(2)} &= 2\sqrt{2} g_L g_L' g_s [L(1234) - R^*(2143)] \\ &= 2\sqrt{2} g_L g_L' g_s \frac{[14]}{[15][25][5r]} [([25][1r] - [15][2r]) \langle 32 \rangle - [15][5r] \langle 35 \rangle]. \end{aligned} \quad (\text{A.20})$$

Applying the Schouten identity

$$[ij][k\ell] + [ik][\ell j] + [i\ell][jk] = \langle ij \rangle \langle k\ell \rangle + \langle ik \rangle \langle \ell j \rangle + \langle i\ell \rangle \langle jk \rangle = 0 \quad (\text{A.21})$$

we have

$$[25][1r] - [15][2r] = [21][5r] \quad (\text{A.22})$$

so the dependence on the reference vector r cancels and we find

$$A_{LL, L}^{(1)} - A_{LL, L}^{(2)} = 2\sqrt{2} g_L g_L' g_s \frac{\langle 34 \rangle [14]^2}{[15][25]}. \quad (\text{A.23})$$

Here we have used momentum conservation to write $\langle 32 \rangle [21] + \langle 35 \rangle [51] = \langle 34 \rangle [14]$. Similarly

$$\begin{aligned} A_{LL, L}^{(3)} - A_{LL, L}^{(4)} &= 2\sqrt{2} g_L g_L' g_s [R^*(3412) - L(4321)] \\ &= 2\sqrt{2} g_L g_L' g_s \frac{\langle 12 \rangle [14]^2}{[45][35]}. \end{aligned} \quad (\text{A.24})$$

Taking the square moduli gives

$$\begin{aligned} |A_{LL, L}^{(1)} - A_{LL, L}^{(2)}|^2 &= 8 g_L^2 g_L'^2 g_s^2 s_{14}^2 \frac{s_{34}}{s_{15} s_{25}}, \\ |A_{LL, L}^{(3)} - A_{LL, L}^{(4)}|^2 &= 8 g_L^2 g_L'^2 g_s^2 s_{14}^2 \frac{s_{12}}{s_{35} s_{45}}. \end{aligned} \quad (\text{A.25})$$

The other helicity amplitudes give similar contributions, with the factor of s_{14}^2 replaced by the corresponding term in the final column of Table 6. Thus the overall spin-averaged matrix element squared is

$$\overline{\sum} \mathcal{M}^{\text{sing}} = 2C_F g_s^2 \left[(g_L^2 g_L'^2 + g_R^2 g_R'^2)(s_{14}^2 + s_{23}^2) + (g_L^2 g_R'^2 + g_R^2 g_L'^2)(s_{13}^2 + s_{24}^2) \right] \left(\frac{s_{34}}{s_{15}s_{25}} + \frac{s_{12}}{s_{35}s_{45}} \right). \quad (\text{A.26})$$

In the colour octet (adjoint representation) case, the reference vector dependence cancels for any value of N . Using the colour factors in Table 1, in place of (A.26) we have

$$\overline{\sum} \mathcal{M}^{\text{oct}} = 2g_s^2 \left[(g_L^2 g_L'^2 + g_R^2 g_R'^2)(s_{14}^2 + s_{23}^2) + (g_L^2 g_R'^2 + g_R^2 g_L'^2)(s_{13}^2 + s_{24}^2) \right] \sum_{i < j} C_{ij} \frac{s_{k\ell}}{s_{i5}s_{j5}}, \quad (\text{A.27})$$

where $k, \ell \neq i, j, 5$.

A.2 QCD amplitudes

The QCD helicity amplitudes for one gluon emission are as in the octet case above, except for the following changes:

- The couplings are $g_{L,R} = g'_{L,R} = g_s$.
- The gluon propagator gives a factor of $1/s_{34}$ in $A_{hh',h''}^{(1,2)}$ and $1/s_{12}$ in $A_{hh',h''}^{(3,4)}$.
- There is an extra contribution $A_{hh',h''}^{(g)}/s_{12}s_{34}$ from the diagram with a gluon emitted from the gluon propagator.

For $hh' = LL$, the numerator of the extra contribution is

$$\begin{aligned} A_{LL,L}^{(g)} &= 2\sqrt{2}g_s^3[14] \left(\frac{\langle 53 \rangle [3r] + \langle 54 \rangle [4r]}{[5r]} \langle 32 \rangle - \langle 35 \rangle \langle 52 \rangle \right) \equiv 2\sqrt{2}g_s^3 G(1234), \\ A_{LL,R}^{(g)} &= 2\sqrt{2}g_s^3 \langle 32 \rangle \left(\frac{\langle r3 \rangle [35] + \langle r4 \rangle [45]}{\langle r5 \rangle} [14] - [15][54] \right) = 2\sqrt{2}g_s^3 G^*(2143), \end{aligned} \quad (\text{A.28})$$

with permutations for the other helicities as shown in Table 6.

The colour factors are such that emissions from lines 3 and 4 receive an extra contribution $A_{hh',h''}^{(g)}/2s_{12}s_{34}$, while those from 1 and 2 receive the opposite contribution. Therefore the extra contribution cancels in the $i, j = 1, 2$ and $3, 4$ terms of Eq. (A.27) but not in the others. Consider for example the term involving

$$A_{LL,L}^{(1)}/s_{34} - A_{LL,L}^{(4)}/s_{12} - A_{LL,L}^{(g)}/s_{12}s_{34} = 2\sqrt{2} \frac{g_s^3}{s_{12}s_{34}} [L(1234)s_{12} - L(4321)s_{34} - G(1234)]. \quad (\text{A.29})$$

Now $s_{12} = s_{34} + s_{35} + s_{45}$, so this is equal to

$$2\sqrt{2} \frac{g_s^3}{s_{12}s_{34}} \{ L[(1234) - L(4321)]s_{34} + L(1234)(s_{35} + s_{45}) - G(1234) \}. \quad (\text{A.30})$$

We want to show that this is independent of the reference vector p_r . The first term in the curly bracket is independent, by the argument in the previous subsection. The remainder involves

$$L(1234)(s_{35} + s_{45}) - G(1234) = \frac{\langle 32 \rangle [14]}{[15][5r]} \left\{ [1r](\langle 53 \rangle [35] + \langle 54 \rangle [45]) - [15](\langle 53 \rangle [3r] + \langle 54 \rangle [4r]) \right\} + \langle 35 \rangle \langle 52 \rangle [14]. \quad (\text{A.31})$$

Applying the Schouten identity, the r -dependence cancels and we find

$$L(1234)(s_{35} + s_{45}) - G(1234) = \frac{[14]}{[15]} (\langle 32 \rangle \langle 25 \rangle [21] + \langle 35 \rangle \langle 52 \rangle [15]), \quad (\text{A.32})$$

where we have used momentum conservation to write $\langle 53 \rangle [31] + \langle 54 \rangle [41] = \langle 25 \rangle [21]$. Similarly, the extra term cancels the r -dependence of the other terms in which it appears. In fact, it ensures that the simple correspondence between the helicity contributions and the terms in the last column of Table 6 remains valid. Corresponding to Eq. (A.27) we have

$$\overline{\sum} \mathcal{M}^{\text{QCD}} = 4 \frac{g_s^6}{s_{12}s_{34}} (s_{14}^2 + s_{23}^2 + s_{13}^2 + s_{24}^2) \sum_{i < j} C_{ij} \frac{s_{ij}}{s_{i5}s_{j5}}. \quad (\text{A.33})$$

A.3 Interference

Given the helicity amplitudes listed above, it is straightforward to combine the QCD and octet four-fermion contributions taking into account their interference. The combined amplitudes take the form (showing the couplings explicitly)

$$\begin{aligned} A_{hh',h''}^{(i)} \left(g_h g_{h'}' + \frac{g_s^2}{s_{34}} \right) - A_{hh',h''}^{(g)} \frac{g_s^2}{2s_{12}s_{34}} \quad (i = 1, 2) \\ A_{hh',h''}^{(i)} \left(g_h g_{h'}' + \frac{g_s^2}{s_{12}} \right) + A_{hh',h''}^{(g)} \frac{g_s^2}{2s_{12}s_{34}} \quad (i = 3, 4). \end{aligned} \quad (\text{A.34})$$

Consider first the $i = 1, 2$ contribution:

$$\begin{aligned} \overline{\sum} \left| g_h g_{h'}' (A_{hh',h''}^{(1)} - A_{hh',h''}^{(2)}) + \frac{g_s^2}{s_{12}s_{34}} (A_{hh',h''}^{(1)} s_{12} - A_{hh',h''}^{(2)} s_{34}) \right|^2 \\ = \overline{\sum} \left\{ |A^{\text{oct}}|^2 + |A^{\text{QCD}}|^2 + 2 \frac{g_h g_{h'}' g_s^2}{s_{12}s_{34}} \text{Re} \left[(A_{hh',h''}^{(1)} - A_{hh',h''}^{(2)})^* (A_{hh',h''}^{(1)} s_{12} - A_{hh',h''}^{(2)} s_{34}) \right] \right\}. \end{aligned} \quad (\text{A.35})$$

The interference terms give

$$2 \frac{g_s^4}{s_{12}s_{34}} \left[(g_L g_L' + g_R g_R') (s_{14}^2 + s_{23}^2) + (g_L g_R' + g_R g_L') (s_{13}^2 + s_{24}^2) \right] \sum_{i < j} C_{ij} \frac{x_{ij}}{s_{i5}s_{j5}}, \quad (\text{A.36})$$

where $x_{12} = x_{34} = 2s_{12}s_{34}$. In the other cases there is a contribution from $A_{hh',h''}^{(g)}$ and the results are slightly more complicated:

$$\begin{aligned} x_{13} = x_{24} = s_{14}s_{23} - s_{13}s_{24} - s_{12}s_{34}, \\ x_{14} = x_{23} = s_{13}s_{24} - s_{14}s_{23} - s_{12}s_{34}. \end{aligned} \quad (\text{A.37})$$

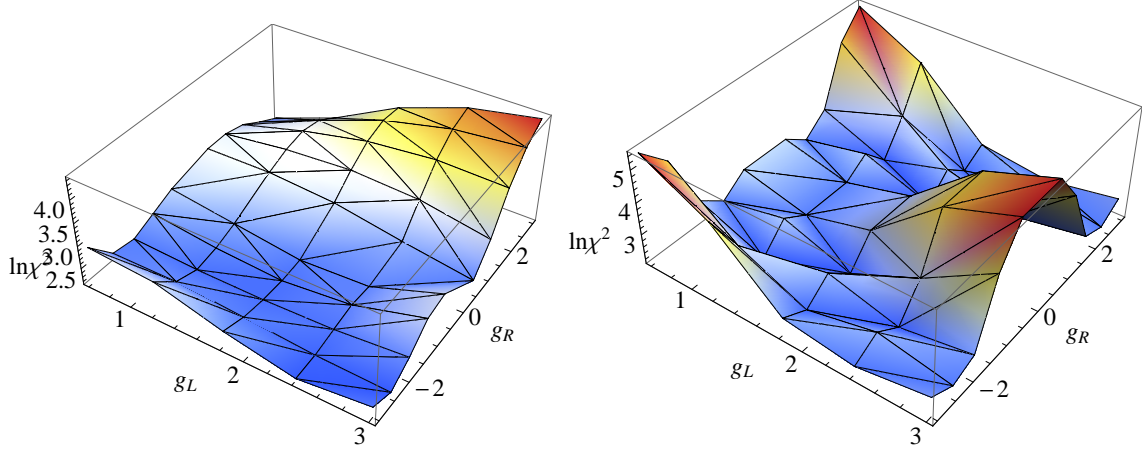


Figure 10: As in Fig. 3, but using massless matrix elements instead of the massive ones.

A.4 Results

Figure 10 shows the results of using the massless matrix elements derived above instead of the massive ones in the fits to the $t\bar{t}$ transverse momentum dependence of the asymmetry. Here we used the massive kinematics for each phase space point, and computed the massless matrix elements from the actual massive s_{ij} values according to the expressions given. Comparing with Fig. 3, we see that the essential qualitative features of the predictions are captured by this simple prescription.

References

- [1] **DØ** Collaboration, V. M. Abazov *et. al.*, *First measurement of the forward-backward charge asymmetry in top quark pair production*, *Phys. Rev. Lett.* **100** (2008) 142002, [[arXiv:0712.0851](#)].
- [2] **CDF** Collaboration, T. Aaltonen *et. al.*, *Forward-Backward Asymmetry in Top Quark Production in $p\bar{p}$ Collisions at $\sqrt{s}=1.96$ TeV*, *Phys. Rev. Lett.* **101** (2008) 202001, [[arXiv:0806.2472](#)].
- [3] **CDF** Collaboration, T. Aaltonen *et. al.*, *Evidence for a Mass Dependent Forward-Backward Asymmetry in Top Quark Pair Production*, *Phys. Rev.* **D83** (2011) 112003, [[arXiv:1101.0034](#)].
- [4] **DØ** Collaboration, V. M. Abazov *et. al.*, *Forward-backward asymmetry in top quark-antiquark production*, *Phys.Rev.* **D84** (2011) 112005, [[arXiv:1107.4995](#)].
- [5] J. F. Kamenik, J. Shu, and J. Zupan, *Review of New Physics Effects in t - t bar Production*, *Eur.Phys.J.* **C72** (2012) 2102, [[arXiv:1107.5257](#)].
- [6] S. Westhoff, *Top-Quark Asymmetry – A New Physics Overview*, *PoS EPS-HEP2011* (2011) 377, [[arXiv:1108.3341](#)].
- [7] J. Aguilar-Saavedra, *Overview of models for the t t bar asymmetry*, *Nuovo Cim.* **C035N3** (2012) 167–172, [[arXiv:1202.2382](#)].

- [8] W. Hollik and D. Pagani, *The electroweak contribution to the top quark forward-backward asymmetry at the Tevatron*, *Phys.Rev.* **D84** (2011) 093003, [[arXiv:1107.2606](#)].
- [9] J. H. Kuhn and G. Rodrigo, *Charge asymmetries of top quarks at hadron colliders revisited*, *JHEP* **1201** (2012) 063, [[arXiv:1109.6830](#)].
- [10] W. Bernreuther and Z.-G. Si, *Top quark and leptonic charge asymmetries for the Tevatron and LHC*, *Phys.Rev.* **D86** (2012) 034026, [[arXiv:1205.6580](#)].
- [11] **CDF** Collaboration, T. A. Aaltonen *et. al.*, *Measurement of the leptonic asymmetry in $t\bar{t}$ events produced in $p\bar{p}$ collisions at $\sqrt{s} = 1.96$ TeV*, [arXiv:1308.1120](#).
- [12] **DØ** Collaboration, V. M. Abazov *et. al.*, *Measurement of the asymmetry in angular distributions of leptons produced in dilepton $t\bar{t}$ final states in $p\bar{p}$ collisions at $\sqrt{s} = 1.96$ TeV*, [arXiv:1308.6690](#).
- [13] **CDF** Collaboration, T. Aaltonen *et. al.*, *Measurement of the top quark forward-backward production asymmetry and its dependence on event kinematic properties*, *Phys.Rev.* **D87** (2013) 092002, [[arXiv:1211.1003](#)].
- [14] S. Hoeche, J. Huang, G. Luisoni, M. Schoenherr, and J. Winter, *Zero and one jet combined NLO analysis of the top quark forward-backward asymmetry*, *Phys.Rev.* **D88** (2013) 014040, [[arXiv:1306.2703](#)].
- [15] Y. L. Dokshitzer, V. A. Khoze, S. Troian, and A. H. Mueller, *QCD Coherence in High-Energy Reactions*, *Rev.Mod.Phys.* **60** (1988) 373.
- [16] P. Skands, B. Webber, and J. Winter, *QCD Coherence and the Top Quark Asymmetry*, *JHEP* **1207** (2012) 151, [[arXiv:1205.1466](#)].
- [17] J. Aguilar-Saavedra, *Effective four-fermion operators in top physics: A Roadmap*, *Nucl.Phys.* **B843** (2011) 638–672, [[arXiv:1008.3562](#)].
- [18] C. Degrande, J.-M. Gerard, C. Grojean, F. Maltoni, and G. Servant, *Non-resonant New Physics in Top Pair Production at Hadron Colliders*, *JHEP* **1103** (2011) 125, [[arXiv:1010.6304](#)].
- [19] D. Y. Shao, C. S. Li, J. Wang, J. Gao, H. Zhang, *et. al.*, *Model independent analysis of top quark forward-backward asymmetry at the Tevatron up to $\mathcal{O}(\alpha_S^2/\Lambda^2)$* , *Phys.Rev.* **D84** (2011) 054016, [[arXiv:1107.4012](#)].
- [20] R. Mertig, M. Bohm, and A. Denner, *FEYN CALC: Computer algebraic calculation of Feynman amplitudes*, *Comput.Phys.Commun.* **64** (1991) 345–359.
- [21] R. K. Ellis and J. C. Sexton, *Explicit Formulae for Heavy Flavor Production*, *Nucl. Phys.* **B282** (1987) 642.
- [22] A. D. Martin, W. J. Stirling, R. S. Thorne, and G. Watt, *Parton distributions for the LHC*, *Eur.Phys.J.* **C63** (2009) 189–285, [[arXiv:0901.0002](#)].
- [23] C. Zhang and S. Willenbrock, *Effective-Field-Theory Approach to Top-Quark Production and Decay*, *Phys.Rev.* **D83** (2011) 034006, [[arXiv:1008.3869](#)].
- [24] K. Blum, C. Delaunay, O. Gedalia, Y. Hochberg, S. J. Lee, *et. al.*, *Implications of the CDF $t\bar{t}$ Forward-Backward Asymmetry for Boosted Top Physics*, *Phys.Lett.* **B702** (2011) 364–369, [[arXiv:1102.3133](#)].

- [25] C. Delaunay, O. Gedalia, Y. Hochberg, G. Perez, and Y. Soreq, *Implications of the CDF $t\bar{t}$ Forward-Backward Asymmetry for Hard Top Physics*, *JHEP* **1108** (2011) 031, [[arXiv:1103.2297](#)].
- [26] J. Aguilar-Saavedra and M. Perez-Victoria, *Probing the Tevatron $t\bar{t}$ asymmetry at LHC*, *JHEP* **1105** (2011) 034, [[arXiv:1103.2765](#)].
- [27] J. L. Hewett, J. Shelton, M. Spannowsky, T. M. Tait, and M. Takeuchi, *A_{FB}^t Meets LHC*, *Phys.Rev.* **D84** (2011) 054005, [[arXiv:1103.4618](#)].
- [28] M. Bähr, S. Gieseke, M. A. Gigg, D. Grellscheid, K. Hamilton, *et. al.*, *Herwig++ Physics and Manual*, *Eur.Phys.J.* **C58** (2008) 639–707, [[arXiv:0803.0883](#)]. Program and additional information available from <http://projects.hepforge.org/herwig>.
- [29] K. Arnold, L. d’Errico, S. Gieseke, D. Grellscheid, K. Hamilton, *et. al.*, *Herwig++ 2.6 Release Note*, [[arXiv:1205.4902](#)].
- [30] S. Dittmaier, P. Uwer, and S. Weinzierl, *Hadronic top-quark pair production in association with a hard jet at next-to-leading order QCD: Phenomenological studies for the Tevatron and the LHC*, *Eur.Phys.J.* **C59** (2009) 625–646, [[arXiv:0810.0452](#)].
- [31] K. Melnikov, A. Scharf, and M. Schulze, *Top quark pair production in association with a jet: QCD corrections and jet radiation in top quark decays*, *Phys.Rev.* **D85** (2012) 054002, [[arXiv:1111.4991](#)].